

Turbulent free-surface in self-aerated flows: Superposition of entrapped and entrained air

Matthias Kramer¹ †

¹UNSW Canberra, School of Engineering and Technology (SET), Canberra, ACT 2610, Australia

(Received 24 June 2023; revised 14 Sep 2023; accepted 03 Dec 2023)

The characterisation and the modelling of air concentration distributions in self-aerated free-surface flows has been subject to sustained research interest since the 1970s. Recently, a novel two-state formulation of the structure of a self-aerated flow was proposed by Kramer & Valero [2023 J. Fluid Mech. 966, A37], which physically explains the air concentration through the weak interaction of two canonical flow momentum layers, comprising a Turbulent Boundary Layer (TBL) and a Turbulent Wavy Layer (TWL). The TWL was modelled using a Gaussian error function, assuming that the most dominant contribution are wave troughs. Here, it is shown that air bubbles form an integral part of the TWL, and its formulation is expanded by adopting a superposition principle of entrapped air (waves) and entrained air (bubbles). Combining the superposition principle with the two-state formulation, an expression for the depth-averaged (mean) air concentration is derived, which allows to quantify the contribution of different physical mechanisms to the mean air concentration. Overall, the presented concepts help to uncover new flow physics, thereby contributing fundamentally to our understanding of self-aerated flows.

Key words: channel flow, turbulent flows, bubble dynamics

1. Introduction

Self-aeration is a fascinating flow phenomenon that is frequently observed in high Froude-number open-channel flows (Fig. 1). Such flows are characterised by strong turbulence and neither surface tension nor gravity are able to maintain surface cohesion (Brocchini & Peregrine 2001), causing entrainment of air bubbles into the flow column. These bubbles subsequently break down into a wide range of bubble sizes (Lamarre & Melville 1991; Deike et al. 2016; Deane & Stokes 2002; Chan et al. 2021), and eventually penetrate towards the channel bottom through turbulent diffusion. It is known that entrained air can significantly alter flow properties, thereby leading to flow bulking, drag reduction, cavitation protection, and enhanced gas transfer (Straub & Anderson 1958; Falvey 1990; Gulliver et al. 1990; Kramer et al. 2021).

As such, the characterization and the modelling of air concentration distributions has been subject to sustained research interest over the last decades. Different groups of researchers

† Email address for correspondence: m.kramer@unsw.edu.au

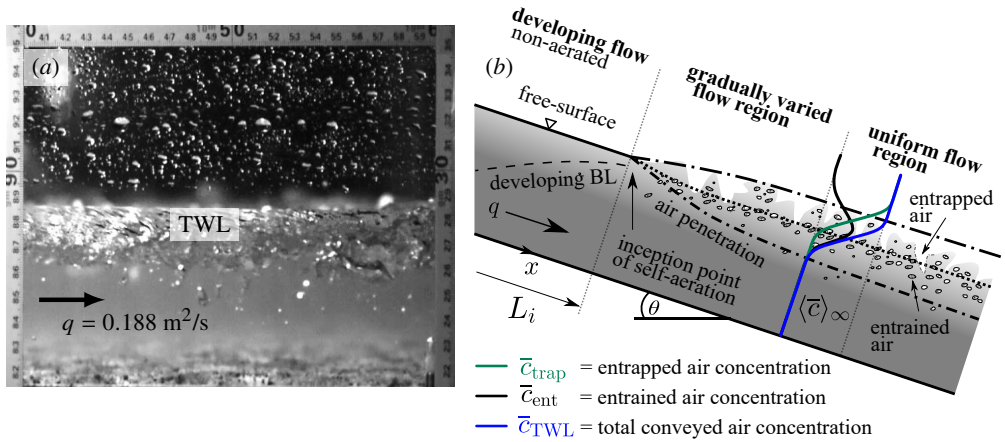


Figure 1: Self-aeration in high Froude-number flows (a) TWL of a flow over a micro-rough channel bed at the Water Research Laboratory (WRL), UNSW Sydney, Australia; specific water flow rate $q = 0.188 \text{ m}^2/\text{s}$, chute angle $\theta = 10.8^\circ$, streamwise distance from invert $x = 6.3 \text{ m}$ to 6.5 m ; image courtesy of Armaghan Severi, adapted with permission (b) schematic of the TWL of a self-aerated flow down a smooth chute, including a differentiation between entrapped, entrained and total conveyed air

have conceptualised the air concentration using single-layer (Rao & Gangadharaiiah 1971; Wood 1991; Chanson & Toombes 2001; Zhang & Chanson 2017; Valero & Bung 2016) or double-layer approaches (Straub & Anderson 1958; Killen 1968; Wei & Deng 2022; Wei et al. 2022). Based on visual observations, various physical processes have been identified in self-aerated flows, comprising generation of free-surface waves, surface disruption, air entrainment, turbulent diffusion of air bubbles, and ejection of droplets. It is argued that single-layer approaches are unable to represent these different flow processes, while good data-driven agreement between single-layer models and measurements has been achieved, which is however at the expense of empirically fitted coefficients. Recently, Kramer & Valero (2023) presented a physically based two-state convolution formulation for the air concentration that is built upon a Turbulent Boundary Layer (TBL) and a Turbulent Wavy Layer (TWL).

It is important to note that none of the previous single-layer or double-layer air concentration conceptualizations have taken into account the contribution of entrapped and entrained air, as depicted in Fig. 1b, which is introduced in the following. In a seminal series of experiments, Killen (1968) investigated surface characteristics of self-aerated flows by deploying a common phase-detection probe as well as a larger-sized conduction probe that dipped in and out of the surface roughness/waves, hereafter referred to as *dipping probe*. Wilhelms & Gulliver (2005) re-analyzed the data of Killen (1968) and pointed out that the dipping probe measured entrapped air, transported between wave crests and troughs, whereas the common phase-detection probe measured a combination of entrapped and entrained air, termed total conveyed air. Although Wilhelms & Gulliver (2005) articulated the need for two measurements, one for entrapped air and one for total conveyed air, no other researchers have deployed a dipping probe since, showing the uniqueness of Killen's (1968) data set.

The key novelty of the present work is the introduction of a superposition principle, which explicitly accounts for entrapped air (waves) and entrained air (bubbles), allowing to quantify the importance of different physical mechanisms to the mean air concentration. In the following, the two-state formulation of Kramer & Valero (2023) is briefly summarised (§

2.1). Thereafter, the superposition principle for the air concentration of the TWL is proposed, demonstrating that entrapped air and entrained air follow a Gaussian error function and a normal distribution, respectively (§ 2.2). The superposition principle is then combined with the two-state convolution in § 2.3, providing the most complete and physically consistent description of the air concentration distribution to date. A bed-normal integration of this expanded formulation allows to differentiate between three different physical mechanisms that contribute to the mean air concentration, comprising entrapped air within the TWL, entrained air within the TWL, and entrained air within the TBL (§ 2.3). The different parameters of the superposition principle as well as the application of the new formulation are assessed against Killen's (1968) data set in § 3, followed by a discussion on model applicability and other limitations (§ 4).

2. Methods

2.1. Two-state convolution

This section provides a brief summary of the governing equations of the two-state convolution model, while more details are presented in Kramer & Valero (2023). The air concentration of the TBL (\bar{c}_{TBL}) is reflected through a solution of the advection diffusion equation for air in water, whereas the air concentration of the TWL (\bar{c}_{TWL}), encompassing bubbles and waves, was found to follow a Gaussian error function (Kramer & Valero 2023)

$$\bar{c}_{\text{TBL}} = \begin{cases} \bar{c}_{\delta/2} \left(\frac{y}{\delta-y}\right)^\beta, & y \leq \delta/2, \\ \bar{c}_{\delta/2} \exp\left(\frac{4\beta}{\delta}\left(y - \frac{\delta}{2}\right)\right), & y > \delta/2, \end{cases} \quad (2.1)$$

$$\bar{c}_{\text{TWL}} = \frac{1}{2} \left(1 + \operatorname{erf}\left(\frac{y - y_{50}}{\sqrt{2}\mathcal{H}}\right)\right), \quad (2.2)$$

where $\bar{c}_{\delta/2}$ is the air concentration at half the boundary layer thickness (δ), y is the bed-normal coordinate, $\beta = \bar{v}_r S_c / \kappa u_*$ is the Rouse number, \bar{v}_r is the bed-normal bubble rise velocity, κ is the van Karman constant, u_* is the friction velocity, and S_c is the turbulent Schmidt number, defined as the ratio of eddy viscosity and turbulent mass diffusivity. Further, \mathcal{H} is a characteristic length-scale that is proportional to the thickness of the TWL, erf is the Gaussian error function, and y_{50} is the mixture flow depth where the total conveyed air concentration is $\bar{c} = 0.5$; note that other mixture flow depths are represented in the same manner, e.g., $y_{90} = y(\bar{c} = 0.9)$. The two-state model assumes a fluctuating interface that separates the TBL and the TWL, and a convolution of the two states with a Gaussian interface probability led to the following expression for the mean air concentration (Krug et al. 2017; Kramer & Valero 2023)

$$\bar{c} = \bar{c}_{\text{TBL}}(1 - \Gamma) + \bar{c}_{\text{TWL}}\Gamma, \quad (2.3)$$

with

$$\Gamma(y; y_\star, \sigma_\star) = \frac{1}{2} \left(1 + \operatorname{erf}\left(\frac{y - y_\star}{\sqrt{2}\sigma_\star}\right)\right), \quad (2.4)$$

where y_\star is the time-averaged interface position and σ_\star is its standard deviation. It is noted that the two-state formulation [Eq. (2.3)] has been successfully validated against more than 500 air concentration data-sets from literature, hinting at universal applicability. For more information on the development of Eqns. (2.1) to (2.4), as well as on the definition and determination of associated physical model parameters, the reader is referred to Kramer & Valero (2023).

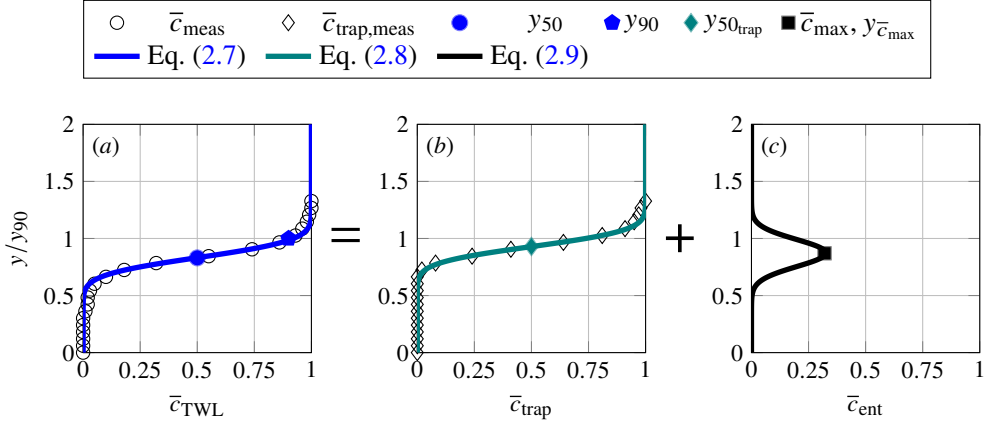


Figure 2: Representation of Killen's (1968) measurements in a self-aerated flow with $q = 0.78 \text{ m}^2/\text{s}$, $\theta = 30^\circ$, and $x = 7.4 \text{ m}$; meas = measured (a) total conveyed air concentration, measured with a common phase-detection probe (b) entrapped air concentration, measured with a dipping probe (c) entrained air concentration, determined through the superposition principle

2.2. Superposition principle (TWL)

Herein, it is hypothesized that the air concentration of the TWL results from a superposition of waves and entrained air bubbles, which was similarly proposed by Wilhelms & Gulliver (2005) for the mean air concentration. To formulate this principle, the focus is set on a flow situation where aeration is confined to the wavy layer, similar to Fig. 1. The entrapped air concentration of the TWL can be interpreted as the probability of encountering entrapped air at a certain location within the flow. In a time-averaged sense, this probability can be expressed as $p(\bar{c}_{\text{trap}}) = \mathcal{V}_{\text{trap}}/\mathcal{V}_{\text{tot}}$, where $\mathcal{V}_{\text{trap}}$ = volume of entrapped air and $\mathcal{V}_{\text{tot}} = \mathcal{V}_{\text{trap}} + \mathcal{V}_{\text{ent}} + \mathcal{V}_{\text{W}}$ = total volume of the mixture, including the volume of entrained air (\mathcal{V}_{ent}) and the volume of water (\mathcal{V}_{W}). The probability of encountering an entrained air bubble within a wave is $p(\bar{c}_{\text{ent}}^* | \bar{c}_{\text{trap}}) = \mathcal{V}_{\text{ent}}/(\mathcal{V}_{\text{ent}} + \mathcal{V}_{\text{W}})$, which is a conditional probability, given that a wave/water phase is present. Considering the two complementary events \bar{c}_{trap} and $(1 - \bar{c}_{\text{trap}})$, the expression for the total conveyed air concentration of the TWL reads

$$\bar{c}_{\text{TWL}} = \bar{c}_{\text{trap}} + (1 - \bar{c}_{\text{trap}}) \bar{c}_{\text{ent}}^*. \quad (2.5)$$

It is recognised that

$$(1 - \bar{c}_{\text{trap}}) \bar{c}_{\text{ent}}^* = \frac{\mathcal{V}_{\text{ent}} + \mathcal{V}_{\text{W}}}{\mathcal{V}_{\text{tot}}} \frac{\mathcal{V}_{\text{ent}}}{\mathcal{V}_{\text{ent}} + \mathcal{V}_{\text{W}}} = \frac{\mathcal{V}_{\text{ent}}}{\mathcal{V}_{\text{tot}}} = \bar{c}_{\text{ent}}, \quad (2.6)$$

where \bar{c}_{ent} is the entrained air concentration, defined as the volume of entrained air bubbles related to the total mixture volume. Combining Eqns. (2.5) and (2.6) leads to the final superposition equation for the TWL (Fig. 2)

$$\bar{c}_{\text{TWL}} = \bar{c}_{\text{trap}} + \bar{c}_{\text{ent}}. \quad (2.7)$$

It is noted that the total conveyed air concentration \bar{c}_{TWL} is described by Eq. (2.2), c.f. Fig. 2a. Valero & Bung (2016) discussed that the entrapped air concentration \bar{c}_{trap} follows an analytical solution of the air-water surface height distribution, which is (also) reflected by

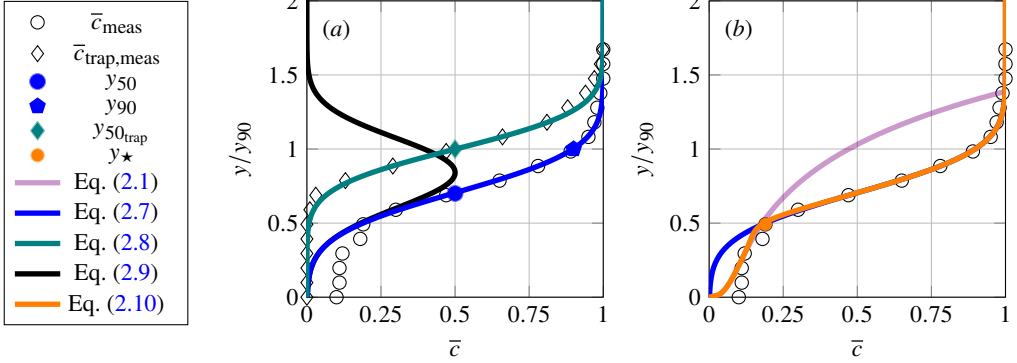


Figure 3: Representation of Killen's (1968) measurements in a self-aerated flow with $q = 0.39 \text{ m}^2/\text{s}$, $\theta = 52.5^\circ$, $x = 3.7 \text{ m}$ (a) superposition principle (b) two-state air concentration convolution

a Gaussian error function (see Fig. 2b)

$$\bar{c}_{\text{trap}} = \frac{1}{2} \left(1 + \operatorname{erf} \left(\frac{y - y_{50\text{trap}}}{\sqrt{2}\mathcal{H}_{\text{trap}}} \right) \right), \quad (2.8)$$

where $y_{50\text{trap}}$ corresponds to the mean water level, and $\mathcal{H}_{\text{trap}}$ is the root-mean-square wave height. Re-arranging Eq. (2.7), an analytical solution for the entrained air concentration can be written as

$$\bar{c}_{\text{ent}} = \bar{c}_{\text{TWL}} - \bar{c}_{\text{trap}} = \frac{1}{2} \left(\operatorname{erf} \left(\frac{y - y_{50}}{\sqrt{2}\mathcal{H}} \right) - \operatorname{erf} \left(\frac{y - y_{50\text{trap}}}{\sqrt{2}\mathcal{H}_{\text{trap}}} \right) \right). \quad (2.9)$$

Figure 2c shows that the entrained air concentration corresponds to the difference of two cumulative Gaussians [Eq. (2.9)], which in turn reflects a Gaussian distribution. Further parameters of interest are the peak entrained air concentration \bar{c}_{max} and its corresponding position $y_{\bar{c}_{\text{max}}}$, which were added to Fig. 2c for completeness. It is emphasized that these two parameters are not necessarily required, as the profile of entrained air (TWL) is mathematically defined by Eq. (2.9).

2.3. Combining both approaches

In § 2.2, the superposition principle was formulated for flow situations where aeration is confined to the wavy layer (pure TWL, compare Figs. 1 and 2). In practice, air bubbles are often diffused deeper into the flow column, one example being shown in Fig. 3, where it is seen that the superposition principle still holds for the TWL (Fig. 3a). In order to explicitly account for the contribution of entrapped and entrained air within the TWL, the two-state convolution [Eq. (2.3)] is combined with the superposition principle [Eq. (2.7)]

$$\bar{c} = (\bar{c}_{\text{trap}} + \bar{c}_{\text{ent}}) \Gamma + \bar{c}_{\text{TBL}}(1 - \Gamma), \quad (2.10)$$

which describes the complete air concentration profile, see Fig. 3b. Further, Eq. (2.10) can be integrated between the channel invert and y_{90} , yielding an expression for the depth-averaged

(mean) air-concentration

$$\langle \bar{c} \rangle = \frac{1}{y_{90}} \int_{y=0}^{y_{90}} \bar{c} \, dy \quad (2.11)$$

$$= \underbrace{\frac{1}{y_{90}} \int_{y=0}^{y_{90}} \bar{c}_{\text{trap}} \Gamma \, dy}_{\langle \bar{c} \rangle_{\text{TWL}_{\text{trap}}}} + \underbrace{\frac{1}{y_{90}} \int_{y=0}^{y_{90}} \bar{c}_{\text{ent}} \Gamma \, dy}_{\langle \bar{c} \rangle_{\text{TWL}_{\text{ent}}}} + \underbrace{\frac{1}{y_{90}} \int_{y=0}^{y_{90}} \bar{c}_{\text{TBL}} (1 - \Gamma) \, dy}_{\langle \bar{c} \rangle_{\text{TBL}}} \quad (2.12)$$

Equation (2.10) represents the most complete and physically consistent description of the air concentration distribution in self-aerated flows to date. Its integrated form [Eq. (2.12)] allows to differentiate between three different physical mechanisms contributing to the mean air concentration, comprising (i) entrapment of air due to free-surface deformations, (ii) entrainment of air due to turbulent forces exceeding gravity and surface tension forces, and (iii) turbulent diffusion of air bubbles into the TBL, represented through $\langle \bar{c} \rangle_{\text{TWL}_{\text{trap}}}$, $\langle \bar{c} \rangle_{\text{TWL}_{\text{ent}}}$, and $\langle \bar{c} \rangle_{\text{TBL}}$, respectively.

3. Results

The application of the superposition principle requires two different measurements, one for entrapped air and one for total conveyed air. Commonly, the total conveyed air has been measured using intrusive phase-detection probes, e.g., Straub & Anderson (1958); Chanson & Toombes (2001); Bung (2009); Severi (2018), whereas entrapped air has rarely been measured, one exception being the smooth chute data from Killen (1968, 20 profiles), to which the expanded formulation of the two-state model is applied. This re-analysis of all 20 profiles is presented in Appendix A, and more details of the original measurements are provided in Table 1. Here, the local Froude-number is defined as $Fr = q / (gd_{\text{eq}}^3)^{1/2}$, with g being the gravitational acceleration and $d_{\text{eq}} = \int_{y=0}^{y_{90}} (1 - \bar{c}) \, dy$ the equivalent clear water flow depth.

Table 1: Experimental flow conditions of Killen (1968); all re-analysed profiles extracted from Wilhelms & Gulliver (1994, Tables B1 to B4); note that the profile number corresponds to Appendix A

Reference (-)	chute type (-)	profile (-)	q (m ² /s)	$\langle \bar{c} \rangle$ (-)	Fr (-)	θ (°)	k_s (mm)
Killen (1968)	smooth	1 to 5	0.39	0.20 to 0.33	9.4 to 11.8	30	0.71
Killen (1968)	smooth	6 to 9	0.78	0.15 to 0.25	10.3 to 12.2	30	0.71
Killen (1968)	smooth	10 to 17	0.39	0.19 to 0.55	14.5 to 21.1	52.5	0.71
Killen (1968)	smooth	18 to 20	0.20	0.35 to 0.42	6.8 to 8.5	30	0.71

k_s = roughness height; chute length = 15.25 m; chute width = 0.46 m

The two free parameters \mathcal{H} and $\mathcal{H}_{\text{trap}}$ of the superposition principle were obtained through least squares fitting. Here, \mathcal{H} was obtained by minimizing the sum of squared differences between measurements and modelled air concentrations within the upper flow region, while the full profile was used for determination of $\mathcal{H}_{\text{trap}}$, as depicted in Fig. 3a. The flow depths y_{50} and $y_{50_{\text{trap}}}$ could be directly extracted from Killen's (1968) data, and were therefore regarded as fixed. Other free and fixed parameters of the two-state convolution (β , y_{\star} , σ_{\star} , $\bar{c}_{\delta/2}$, and δ) had already been determined by Kramer & Valero (2023), and are therefore

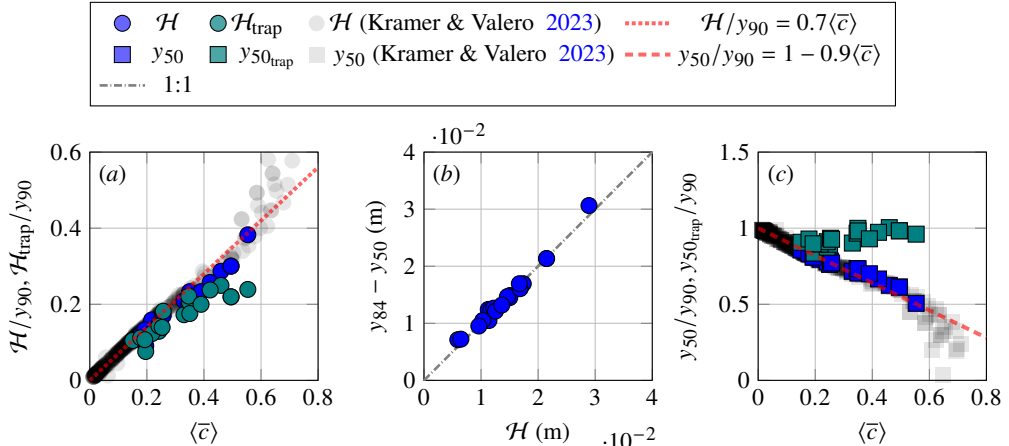


Figure 4: Physical parameters of the TWL for the data of Killen (1968) (a) length scale \mathcal{H} and root-mean-square wave height $\mathcal{H}_{\text{trap}}$ versus mean air concentration (b) three-sigma rule applied to evaluate \mathcal{H} (c) characteristic depths y_{50} and $y_{50_{\text{trap}}}$ versus mean air concentration

not discussed hereafter. In the following, the results of the re-analysis of Killen's (1968) measurements are presented.

3.1. Physical parameters of the TWL

Figure 4a shows the length-scale of the TWL (\mathcal{H}) as well as the root-mean-square wave height ($\mathcal{H}_{\text{trap}}$), both normalised with y_{90} and plotted against the mean air concentration. Similar to the data of Kramer & Valero (2023), there was a linear dependence between \mathcal{H} and $\langle \bar{c} \rangle$. The present analysis reveals that the length scale of the TWL (\mathcal{H}) and the root-mean-square wave height ($\mathcal{H}_{\text{trap}}$) showed some similar trends (Fig. 4a), which implies that \mathcal{H} can provide a rough indication for $\mathcal{H}_{\text{trap}}$, while it is acknowledged that \mathcal{H} may not capture the full complexity of the air-water interface geometry. Further, the empirical three-sigma rule was applied to show that \mathcal{H} corresponded to the difference between the characteristic flow depths y_{84} and y_{50} (Fig. 4b), which was also applicable to $\mathcal{H}_{\text{trap}}$ (not shown). It is worthwhile to mention that roughness effects as well as the streamwise dependence of model parameters are implicitly accounted for in $\langle \bar{c} \rangle$.

As discussed in Kramer & Valero (2023), the normalised flow depth y_{50} was linearly related to the mean air concentration (Fig. 4c). In contrast, the mean water depth $y_{50_{\text{trap}}}$ was found to be less dependent on $\langle \bar{c} \rangle$, and $y_{50_{\text{trap}}}/y_{90}$ became constant for $\langle \bar{c} \rangle > 0.4$ (Fig. 4c). The difference between y_{50} and $y_{50_{\text{trap}}}$ was indicative for the downwards shift of the Gaussian error function for entrapped air, compare Fig. 3a.

3.2. Mean air concentration decomposition

Figure 5a confirms that predicted mean air concentrations [Eq. (2.12)] were in good agreement with measured mean air concentrations, the latter directly evaluated from phase-detection intrusive measurements using Eq. (2.11). Note that Eq. (2.12) was numerically integrated, incorporating the analytical solutions for the \bar{c}_{TBL} [Eq. (2.1)], \bar{c}_{trap} [Eq. (2.8)], \bar{c}_{ent} [Eq. (2.9)], as well as Γ [Eq. (2.4)].

Equation (2.12) allows to differentiate between three different physical mechanisms contributing to the mean air concentration. It was found that $\langle \bar{c} \rangle_{\text{TBL}}$ and $\langle \bar{c} \rangle_{\text{TWL}_{\text{ent}}}$ increased with increasing $\langle \bar{c} \rangle$, whereas the entrapped air concentration of the TWL was approximately constant, at $\langle \bar{c} \rangle_{\text{TWL}_{\text{trap}}} \approx 0.1$ (Fig. 5b; profiles ordered by $\langle \bar{c} \rangle$), which hints at the fact that the

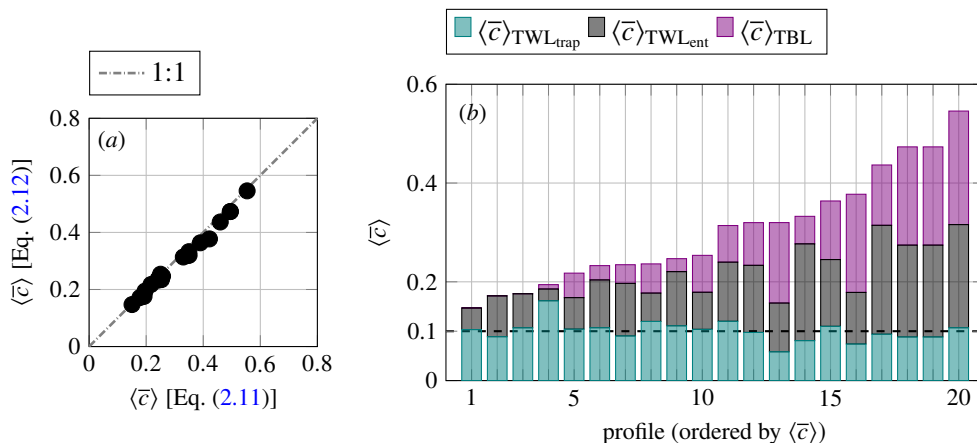


Figure 5: Mean air concentrations derived from Killen's (1968) data (a) measured mean air concentrations versus Eq. (2.12) (b) contribution of different physical mechanisms to the mean air concentration as per Eq. (2.12)

geometry of the (mean) air-water interface of the TWL varied only slightly in Killen's (1968) experiments. Note that a constant entrapped mean air concentration was previously reported by Wilhelms & Gulliver (2005), which is further corroborated by recent computations of the free-surface roughness wavelength distribution in supercritical flows (Valero & Bung 2018, Fig. 12). More generally, the deformation of the free-surface in shallow turbulent flows, and therefore the entrapped air concentration, is known to be driven by various processes, including the interaction of turbulent coherent structures with the water surface, resonant wave growth, and effects of bed topography (Brocchini & Peregrine 2001; Valero & Bung 2016; Muraro et al. 2021). While effects of these different processes on entrapped and entrained air concentrations have not been studied in the past, the current decomposition of the mean air concentration provides a versatile framework that allows to assess the contribution of individual physical mechanisms.

3.3. Streamwise self-aeration development and equilibrium state

In Fig. 5b, the profiles of Killen's (1968) four measurement series (Table 1) were ordered by increasing $\langle \bar{c} \rangle$, which is appropriate to exemplify general trends of $\langle \bar{c} \rangle_{\text{TWL}_{\text{trap}}}$, $\langle \bar{c} \rangle_{\text{TWL}_{\text{ent}}}$, and $\langle \bar{c} \rangle_{\text{TBL}}$ with respect to $\langle \bar{c} \rangle$. To provide more insights on $\langle \bar{c} \rangle$ and its controlling parameters, it is important to point out different distinct regions in self-aerated flows, including the non-aerated developing flow region, the aerated gradually varied flow (GVF) region, and the aerated uniform flow (UF) region (Fig. 1b), which have been described in literature, e.g., Wood (1991); Chanson (1996), amongst others. In the GVF region (Fig. 1b), the mean air concentration $\langle \bar{c} \rangle$ depends on the streamwise location with respect to the inception point of air entrainment (L_i , Fig. 1b), as well as on the slope θ and (similarly) on the Froude-number. In contrast, the mean air concentration in the UF region, termed equilibrium mean air concentration $\langle \bar{c} \rangle_{\infty}$ (Fig. 1b), is known to be solely a function of θ (or Fr) (Hager 1991; Matos 1995).

Figure 6a compares equilibrium air concentrations from Straub & Anderson (1958) with the present re-analysis, showing that Killen's (1968) measurements were taken in the GVF region. Following Wei & Deng (2022), Killen's (1968) mean air concentrations are normalised with their equilibrium value, approximated as $\langle \bar{c} \rangle_{\infty} = 0.75 \sin \theta^{0.75}$ (Hager 1991), and plotted against the dimensionless streamwise coordinate $(x - L_i)/L_i$ (Figs. 6b,c).

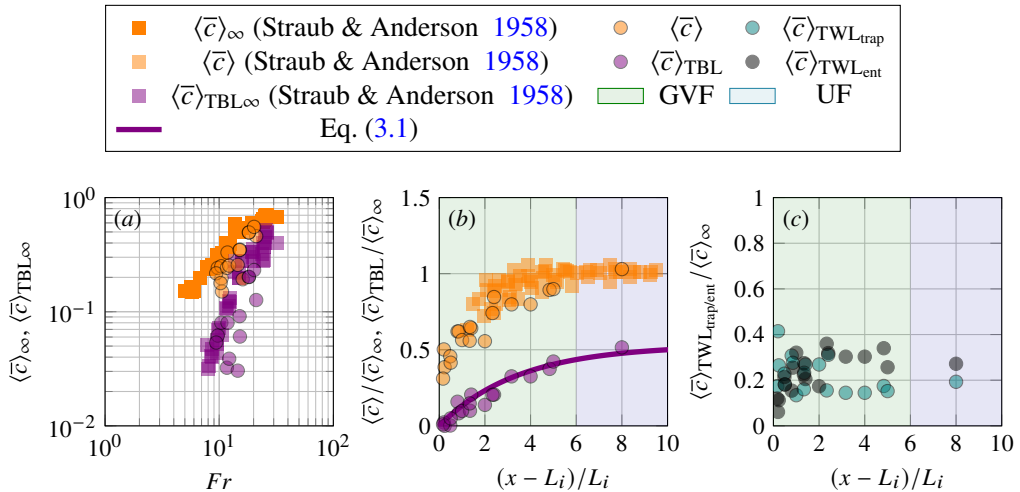


Figure 6: Equilibrium air concentration and streamwise self-aeration development (a) equilibrium air concentrations $\langle \bar{c} \rangle_\infty$ and $\langle \bar{c} \rangle_{\text{TBL}\infty}$ versus Froude-numbers for the data of Straub & Anderson (1958), compared with non-equilibrium concentrations from Killen (1968) (b,c) evolution of depth-averaged (mean) air concentrations in Killen's (1968) high Froude-number flows; GVF = gradually varied flow, UF = uniform flow

This normalisation shows a good collapse of the four different measurement series, thereby demonstrating how the two-state superposition model can be used to finely differentiate between different physical processes in the streamwise decomposition of $\langle \bar{c} \rangle$. The evolution of $\langle \bar{c} \rangle_{\text{TBL}}$ displays asymptotic behaviour towards equilibrium and is well described by an analytical solution of the continuity equation for air in water (Appendix B)

$$\langle \bar{c} \rangle_{\text{TBL}} = \langle \bar{c} \rangle_{\text{TBL}\infty} \left(1 - \exp \left(-\frac{u_r \cos \theta}{q} (x - L_i) \right) \right), \quad (3.1)$$

where $\langle \bar{c} \rangle_{\text{TBL}\infty}$ is the equilibrium mean air concentration of the TBL, and u_r is the depth-averaged bubble rise velocity. Here, Eq. (3.1) was evaluated for Killen's (1968) data on the 52.5 degree slope, and good agreement with measurements was achieved using $u_r = 0.1$ m/s and $\langle \bar{c} \rangle_{\text{TBL}\infty} = 0.53 \langle \bar{c} \rangle_\infty$ (Fig. 6b). The mean air concentration $\langle \bar{c} \rangle$ similarly approaches equilibrium, and an additional comparison with data from Straub & Anderson (1958) reveals that the length of the GVF region is approximately 4 to 6 times L_i (Fig. 6b). Further, Fig. 6c shows that the trends in $\langle \bar{c} \rangle_{\text{TWL}\text{-trap}}$ and $\langle \bar{c} \rangle_{\text{TWL}\text{-ent}}$ are opposite for $(x - L_i) / L_i \lesssim 2$, which is consistent with experimental observations of free-surface roughness/waves, but no entrained air, upstream of the inception point of free-surface aeration (Felder et al. 2023). In the GVF region, around $(x - L_i) / L_i \gtrsim 2$, the contributions of $\langle \bar{c} \rangle_{\text{TWL}\text{-trap}}$ and $\langle \bar{c} \rangle_{\text{TWL}\text{-ent}}$ become approximately constant, which suggests that equilibrium for the TWL is achieved further upstream than for the TBL. Additional research is required to confirm these findings.

4. Discussion: Model applicability and limitations

In § 2.2, the superposition principle [Eq. (2.7)] was formulated for flow situations where aeration is confined to the wavy layer of a supercritical free-surface flow, i.e., a pure TWL, and it was combined with the two-state convolution [Eq. (2.10)] to account for flows where the air bubble diffusion layer protrudes to the channel bottom, see § 2.3. Therefore, the

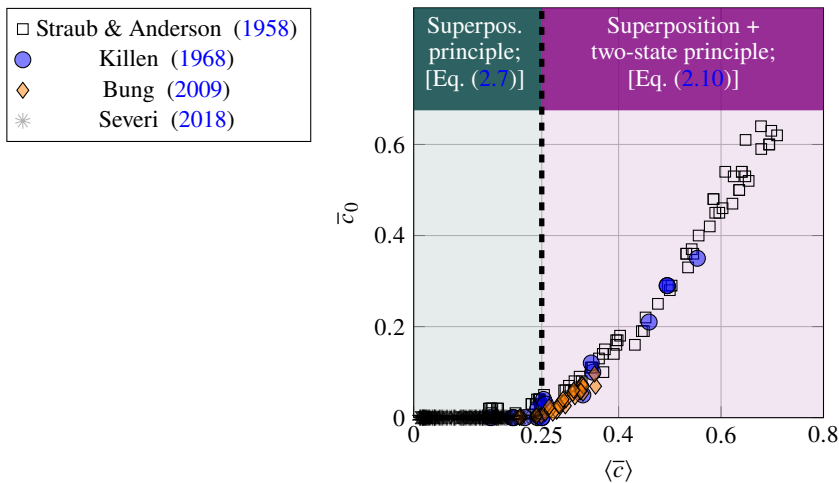


Figure 7: Applicability of the proposed equations for smooth chute flows: variation of \bar{c}_0 versus $\langle \bar{c} \rangle$

bottom air concentration \bar{c}_0 , defined as the air concentration in the vicinity of the solid invert (Hager 1991; Kramer et al. 2021), is a natural choice to exemplify the application range of proposed equations. Figure 7 shows a plot of \bar{c}_0 versus $\langle \bar{c} \rangle$, illustrating that Eq. (2.7) is valid for $\langle \bar{c} \rangle \lesssim 0.25$, while Eq. (2.10) is valid for $\langle \bar{c} \rangle \gtrsim 0.25$. It is noteworthy mentioning that the total conveyed air concentration is fully described by the two-state convolution [Eq. (2.3)] of Kramer & Valero (2023), while the superposition principle provides additional physical insights into the structure of the TWL, given that additional measurements of entrapped air are made.

The model parameters of the extended two-state superposition principle [Eq. (2.10)] are the Rouse number (β), the boundary layer thickness (δ), the air concentration at half the boundary layer thickness ($\bar{c}_{\delta/2}$), the transition/interface parameters y_\star and σ_\star , mixture flow depths y_{50} and $y_{50_{\text{trap}}}$, as well as the length scale of the TWL (\mathcal{H}) and the root-mean-square wave height ($\mathcal{H}_{\text{trap}}$). Of these parameters, y_{50} , $y_{50_{\text{trap}}}$, $\bar{c}_{\delta/2}$, and δ were directly extracted from measurements, whereas β , y_\star , σ_\star , \mathcal{H} , and $\mathcal{H}_{\text{trap}}$ were obtained through fitting. It is acknowledged that the predictive capability for some parameters is currently limited, which is however deemed acceptable, as the aim of the present model is to establish a physically based description of the air concentration distribution, with physical parameters responding to the flow. Further details on \mathcal{H} , $\mathcal{H}_{\text{trap}}$, y_{50} , and $y_{50_{\text{trap}}}$ are presented in Fig. 4, while the interface parameters and the Rouse number range between $\beta = 0.05$ to 1.2, $y_\star/\delta = 0.6$ to 0.9, and $\sigma_\star/\delta = 0.1$ to 0.2 (Kramer & Valero 2023).

As mentioned before, the application of the superposition principle requires two separate measurements, one for entrapped air and one for total conveyed air. Killen (1968) used a common intrusive phase-detection probe for the measurement of total conveyed air, while a larger-sized dipping probe was used for the measurement of entrapped air. It is emphasized that these measurements are unique, and no other researchers have deployed a comparable setup since. Future measurement of entrapped air, either through a measurement setup similar to that of Killen (1968) or via non-intrusive measurement techniques, such as acoustic displacement meters (Cui et al. 2022) or laser time-of-flight or triangulation sensors, are of high relevance to increase our fundamental physical understanding of air-water flow

processes, which is anticipated to lead to an improvement/revision of some existing modelling approaches, e.g., for air-water mass transfer in supercritical flows (Bung & Valero 2018; Kramer 2020).

Lastly, it is stressed that the two-state superposition model has been developed for statistically steady self-aerated flows on steep slopes in prismatic rectangular channels. However, the model can readily be adapted to characterize air concentration distributions of other statistically steady self-aerated flows in prismatic geometries, e.g., hydraulic jumps. The application to unsteady aerated flows, such as breaking waves, is more involved and requires the hundredfold repetition of experiments, followed by an application of ensemble-averaging techniques, see Blenkinsopp & Chaplin (2007); Wuthrich et al. (2022).

5. Conclusion

In this work, a novel superposition principle for entrapped and entrained air within the TWL of a supercritical open-channel flow is presented. The corresponding air concentration distributions for entrapped air and total conveyed air both follow a Gaussian error function, while entrained air is characterized by a Gaussian normal distribution. The free parameters of the mathematical formulation are the root-mean-square wave height and the length scale of the TWL, which are shown to be of similar magnitude and dependent on the mean air concentration. Subsequently, the superposition principle is combined with the two-state convolution of Kramer & Valero (2023), representing the most complete and physical description of the air concentration distribution to date. A bed-normal integration of this combined equation allows to differentiate between three different physical mechanisms that contribute to the mean air concentration, comprising entrapment of air due to free-surface deformations, entrainment of air due to turbulent forces, and turbulent diffusion of air bubbles into the TBL. The subsequent analysis of the streamwise development of these mechanisms suggests that the equilibrium for the TWL is achieved further upstream than for the TBL. While further research is required to confirm this finding, the presented application nicely demonstrates how the two-state superposition model can be used to uncover new flow physics in self-aerated flows. It is acknowledged that only a limited data set was analysed herein, which is because the quantification of entrapped air requires specific flow measurement instrumentation, i.e., a dipping probe.

Overall, it is anticipated that the presented theory holds for a wide range of high Froude-number self-aerated flows, encompassing the range tested by Straub & Anderson (1958, $5 \lesssim Fr \lesssim 32$). A meaningful extension of this work would comprise a thorough development/testing of new sensors for the non-intrusive measurement of entrapped air, as well as the development of advanced phase-detection signal processing techniques that allow to discriminate between entrapped and entrained air. These developments are to be followed by detailed investigations on the functional dependence between model parameters and flow/geometric properties, including bottom-surface roughness, friction velocity, flow depth, as well as other statistical measures of bulk flow and turbulence. A better understanding of the underlying physics of self-aerated flows will enable the formulation and implementation of more physically consistent numerical models for air entrainment and transport.

Acknowledgements. I would like to thank Dr Daniel Valero (Karlsruhe Institute of Technology, KIT) for fruitful discussions, Prof Daniel Bung (FH Aachen) for proof-reading and sharing of data sets, and lastly Dr Armaghan Severi (Manly Hydraulics Laboratory) for sharing her images.

Funding. This research received no specific grant from any funding agency, commercial or not-for-profit sectors.

Declaration of interests. The author reports no conflict of interest.

Data availability statement. All data, models, or code that support the findings of this study are available from the corresponding author upon reasonable request.

Author ORCID. M. Kramer, <https://orcid.org/0000-0001-5673-2751>

REFERENCES

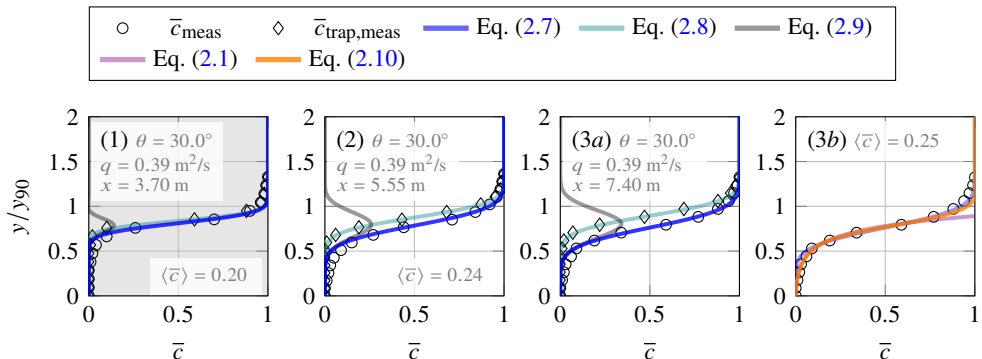
- BLENKINSOPP, C. E. & CHAPLIN, D. H. 2007 Void fraction measurements in breaking waves. *Proc. R. Soc. A* **463**, 3151–3170.
- BROCCHINI, M. & PEREGRINE, D. H. 2022 The dynamics of strong turbulence at free surfaces. Part 1. Description. *J. Fluid Mech.* **449**, 225–254.
- BUNG, D. 2009 Zur selbstbelüfteten Gerinneströmung auf Kaskaden mit gemäßigter Neigung (in German). Phd Thesis, University of Wuppertal.
- BUNG, D. B. & VALERO, D. 2018 Re-aeration on stepped spillways with special consideration of entrained and entrapped air. *Geosci.* **8**, 333.
- CHAN, W. R. C. AND JOHNSON, P. L. AND MOIN, P. 2021 The turbulent bubble break-up cascade. Part 1. Theoretical development. *J. Fluid Mech.* **912**, A42.
- CHANSON, H. 1996 Air bubble-entrainment in free surface turbulent shear flows. Academic Press.
- CHANSON, H. & TOOMBES, L. 2001 Experimental investigations of air entrainment in transition and skimming flows down a stepped chute. Application to embankment overflow stepped spillways. *Research Report No. CE158*. Dept. of Civil Engineering, The University of Queensland, Brisbane.
- CUI, H. AND FELDER, S. AND KRAMER, M. 2022 Non-intrusive measurements of air-water flow properties in supercritical flows down grass-lined spillways. In *Proceedings of the 9th IAHR International Symposium on Hydraulic Structures 24-27 October 2022*, IIT Roorkee, Roorkee, India
- DEIKE, L. AND MELVILLE, K. AND POPINET, S. 2016 Air entrainment and bubble statistics in breaking waves. *J. Fluid Mech.* **801**, 91–129.
- DEANE, G. B. & STOKES, M D. 2002 Scale dependence of bubble creation mechanisms in breaking waves. *Nature* **418** (6900), 839–844.
- FALVEY, H. T. 1990 Cavitation in chutes and spillways. Engineering Monograph No. 42. United States Department of the Interior, Bureau of Reclamation
- FELDER, S. AND SEVERI, A. AND KRAMER, M. 2022 Self-aeration and flow resistance in high-velocity flows down spillways with micro-rough invert. *J. Hydraul. Engng* **149** (6), 04023011.
- GULLIVER, J. S., THENE, J. R., AND RINDELS, A. J. 1990 Indexing gas transfer in self-aerated flows. *J. Environ. Engng* **116** (3), 503–523.
- HAGER, W. H 1991 Uniform aerated chute flow. *J. Hydraul. Engng* **117** (4), 528–533.
- KILLEN, J. M. 1968 The surface characteristics of self aerated flow in steep channels. Phd Thesis, *University of Minnesota*, Minneapolis, MN.
- KRAMER, M. 2020 Air-water flows at hydraulic structures: Experimental investigations of interfacial characteristics and air-water mass transfer. *Technical Report No. KR 4872/2-1*, DFG Research Fellowship.
- KRAMER, M. AND FELDER, S. AND HOHERMUTH, B. AND VALERO, D. 2021 Drag reduction in aerated chute flow: Role of bottom air concentration. *J. Hydraul. Engng* **147** (11), 04021041.
- KRAMER, M. & VALERO, D. 2023 Linking turbulent waves and bubble diffusion in self-aerated open-channel flows: Two-state air concentration. *J. Fluid Mech.* **966**, A37.
- KRUG, D. AND PHILIP, J. AND MARUSIC, I. 2017 Revisiting the law of the wake in wall turbulence. *J. Fluid Mech.* **811**, 421–435.
- MATOS, J. 1995 Discussion of "Air concentration distribution in self-aerated flow" by N.R. Afshar, G.L. Asawa and K.G. Ranga Raju. *J. Hydraul. Res.* **33**, 589–592.
- MURARO, F. AND DOLCETTI, G. AND NICHOLS, A. AND TAIT, S. J. AND HOROSHENKOV, V. K. 2021 Free-surface behaviour of shallow turbulent flows. *J. Hydraul. Res.* **59**, 1–20.
- RAO, N.S.L. & GANGADHARAIHAH, T. 1971 Distribution characteristics of self-aerated flows. In *Characteristics of self-aerated free-surface flows. water and waste water/current research and practice* **10**, 119–161.
- LAMARRE, E. & MELVILLE, W. K. 1991 Air entrainment and dissipation in breaking waves. *Nature* **351**, 469–472.
- SEVERI, A. 2018 Aeration performance and flow resistance in high-Velocity flows over moderately sloped

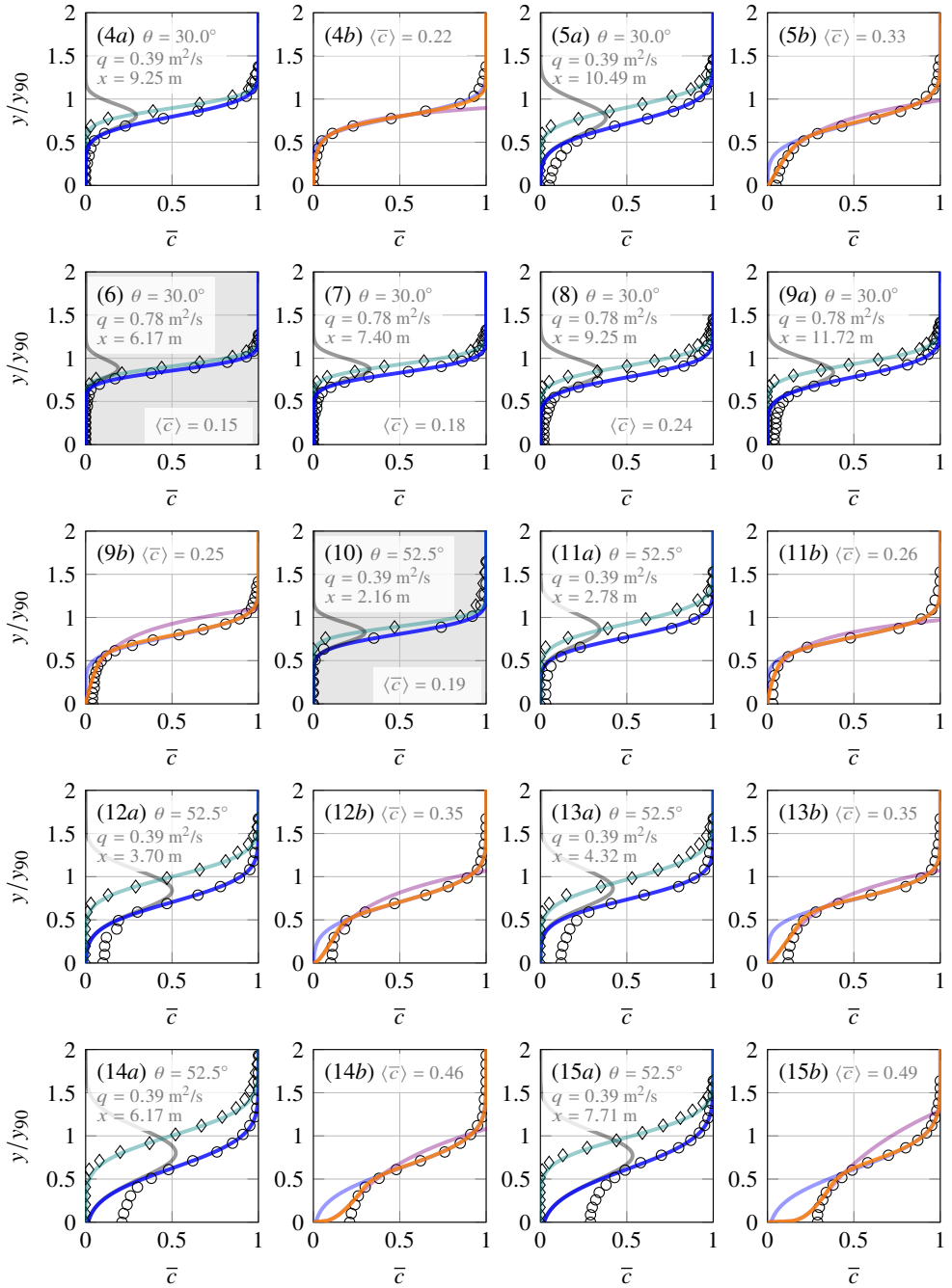
spillways with micro-rough bed. Phd Thesis, Water Research Laboratory, School of Civil and Environmental Engineering, UNSW Sydney.

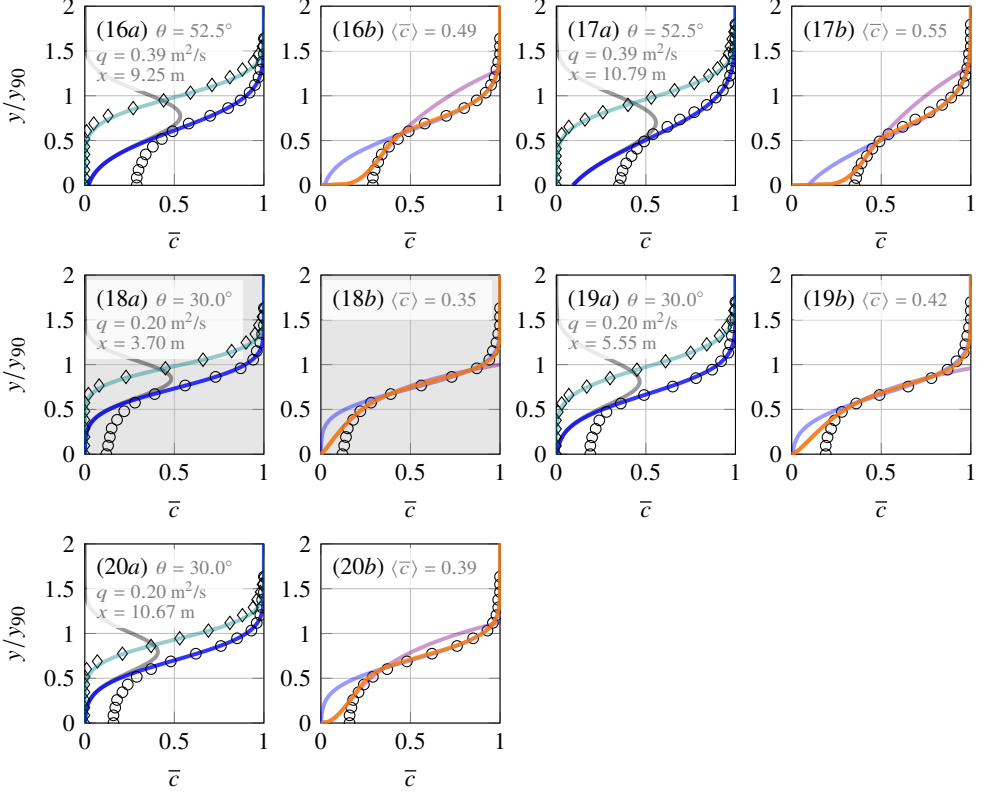
- STRAUB, L. & ANDERSON, A. G. 1958 Experiments on self-aerated flow in open channels. *J. Hydraul. Div.* **84** (7), 1–35.
- VALERO, D. & BUNG, D. 2016 Development of the interfacial air layer in the non-aerated region of high-velocity spillway flows. Instabilities growth, entrapped air and influence on the self-aeration onset. *Int. J. Multiphase Flow* **84**, 66–74.
- VALERO, D. & BUNG, D. 2018 Reformulating self-aeration in hydraulic structures: Turbulent growth of free surface perturbations leading to air entrainment. *Int. J. Multiphase Flow* **100**, 127–142.
- WEI, W. AND DENG, J. 2022 Free surface aeration and development dependence in chute flows. *Sci. Rep.* **12**, 1477.
- WEI, W. AND XU, W. AND DENG, J. AND GUO, Y. 2022 Self-aeration development and fully cross-sectional air diffusion in high-speed open channel flows. *J. Hydraul. Res.* **60** (3), 445–459.
- WILHELMS, S. AND GULLIVER, J. S. 1994 Self-aerated flows on corps of engineers spillways. *Technical Report W-94-2, US Army Corps of Engineers, Waterways Experiment Station.*
- WILHELMS, S. AND GULLIVER, J. S. 2005 Bubbles and waves description of self-aerated spillway flow. *J. Hydraul. Res.* **43** (5), 522–531.
- WOOD, I. 1985 Air water flows. In *Proceedings of the 21st IAHR Congress, Melbourne, Australia, 19-23 August 1985*
- WOOD, I. 1991 Free-surface air entrainment on spillways. In *Air entrainment in free-surface flows - IAHR Hydraulic Structures Design Manual* CRC Press.
- WHUTRICH, D. AND SHI, R. AND CHANSON, H. 2022 Ensemble-statistical approach in the measurement of air–water flow properties in highly unsteady breaking bores. *Rev. Sci. Instrum.* **93**, 054502.
- ZHANG, G. AND CHANSON, H. 2017 Self-aeration in the rapidly- and gradually-varying flow regions of steep smooth and stepped spillways. *Environ. Fluid Mech.* **17**, 27–46.

Appendix A. Re-analysis of Killen’s (1968) measurements

This appendix presents the application of the combined superposition two-state formulation to 20 concentration profiles of Killen’s (1968) data set, with corresponding flow conditions indicated in Table 1. Each measured profile with $\langle \bar{c} \rangle \gtrsim 0.25$ is represented by two sub-figures. In the first sub-figure (index *a*), the superposition principle is plotted with its corresponding Eqns. [(2.8), (2.9), (2.7)], together with the profile number, chute angle (θ), specific discharge (q), and streamwise distance (x in m) from the upstream crest. Each second sub-figure (index *b*) contains plots of the two-state formulation [Eqns. (2.1), (2.7), (2.10)], including the mean air concentration. For $\langle \bar{c} \rangle \lesssim 0.25$, the air concentration distribution is characterised by the superposition principle alone, and only the first sub-figure is plotted (index dropped). The numbering of the profiles increases with streamwise distance for each test series, as per Table 1, and the background of every first profile of the four series is shaded in gray.







Appendix B. Streamwise evolution of $\langle \bar{c} \rangle_{\text{TBL}}$

To develop an equation for the streamwise evolution of $\langle \bar{c} \rangle_{\text{TBL}}$, the continuity equation for entrained air within the TBL is written (Wood 1985)

$$\frac{d(q_{a\text{TBL}})}{dx} = v_e - \langle \bar{c} \rangle_{\text{TBL}} u_r \cos \theta, \quad (\text{B } 1)$$

where $q_{a\text{TBL}}$ is the specific air flow rate of the TBL per unit width, v_e is the entrainment velocity of air into the TBL, and $u_r \cos \theta$ represents detrainment of air, with u_r being a depth-averaged rise velocity of air bubbles. It is noted that previous researchers used the total air flow rate q_a instead of $q_{a\text{TBL}}$, which however is thought to be incorrect, as the volume of entrapped air, for example in the developing non-aerated region, is not balanced by rising air bubbles. Similar to Wood (1985), it is now assumed $q_{a\text{TBL}}/q \approx \langle \bar{c} \rangle_{\text{TBL}}$; note that this assumption represents a simplification, and more elaborate relationships for $q_{a\text{TBL}}/q$ may be used, see Wood (1991); Chanson (1996), which however would not lead to an explicit solution. Substitution of $q_{a\text{TBL}}/q \approx \langle \bar{c} \rangle_{\text{TBL}}$ into Eq. (B 1) leads to

$$q \frac{d\langle \bar{c} \rangle_{\text{TBL}}}{dx} = v_e - \langle \bar{c} \rangle_{\text{TBL}} u_r \cos \theta. \quad (\text{B } 2)$$

In the uniform flow region (Fig. 1), streamwise gradients vanish, implying that Eq. (B 2) simplifies to

$$0 = v_{e\infty} - \langle \bar{c} \rangle_{\text{TBL}\infty} u_{r\infty} \cos \theta, \quad (\text{B } 3)$$

where $v_{e\infty}$, $\langle\bar{c}\rangle_{\text{TBL}\infty}$, and $u_{r\infty}$ are the entrainment velocity, mean air concentration, and bubble rise velocity in the uniform flow region. Equation (B 3) is now subtracted from Eq. (B 2), further assuming $v_e \approx v_{e\infty}$ and $u_r \approx u_{r\infty}$

$$q \frac{d\langle\bar{c}\rangle_{\text{TBL}}}{dx} = u_r \cos \theta (\langle\bar{c}\rangle_{\text{TBL}\infty} - \langle\bar{c}\rangle_{\text{TBL}}). \quad (\text{B } 4)$$

Separating variables

$$\frac{1}{\langle\bar{c}\rangle_{\text{TBL}\infty} - \langle\bar{c}\rangle_{\text{TBL}}} d\langle\bar{c}\rangle_{\text{TBL}} = \frac{u_r \cos \theta}{q} dx, \quad (\text{B } 5)$$

and integrating between the inception point of air entrainment ($x = L_i$) and an arbitrary downstream location

$$\int_0^{\langle\bar{c}\rangle_{\text{TBL}}} \frac{1}{\langle\bar{c}\rangle_{\text{TBL}\infty} - \langle\bar{c}\rangle_{\text{TBL}}} d\langle\bar{c}\rangle_{\text{TBL}} = \frac{u_r \cos \theta}{q} \int_{x=L_i}^x dx, \quad (\text{B } 6)$$

yields the following solution

$$\ln \left(\frac{\langle\bar{c}\rangle_{\text{TBL}\infty}}{\langle\bar{c}\rangle_{\text{TBL}\infty} - \langle\bar{c}\rangle_{\text{TBL}}} \right) = \frac{u_r \cos \theta}{q} (x - L_i), \quad (\text{B } 7)$$

where the lower limit of the integral on the LHS (left-hand side) of Eq. (B 6) corresponds to the entrained air concentration at the inception point, which per definition $\langle\bar{c}\rangle_{\text{TBL}}(x = L_i) = 0$. Equation (B 7) can be re-arranged/simplified to obtain the following analytical expression for the streamwise development of $\langle\bar{c}\rangle_{\text{TBL}}$

$$\langle\bar{c}\rangle_{\text{TBL}} = \langle\bar{c}\rangle_{\text{TBL}\infty} \left(1 - \exp \left(-\frac{u_r \cos \theta}{q} (x - L_i) \right) \right). \quad (\text{B } 8)$$

This equation provides a simple method to characterise the increase of the mean air concentration of the TBL as function of the equilibrium air concentration ($\langle\bar{c}\rangle_{\text{TBL}\infty}$), depth-averaged bubble rise velocity (u_r), slope (θ), specific water flow rate (q), and the streamwise distance from the inception point of air entrainment ($x - L_i$). Substituting $q = \langle\bar{u}\rangle_i d_i$, with $\langle\bar{u}\rangle_i$ and d_i being the mean water velocity and the water depth at the inception point, Wilhelms & Gulliver's (2005, Eq. 4) empirical relationship can be recovered

$$\langle\bar{c}\rangle_{\text{TBL}} = \langle\bar{c}\rangle_{\text{TBL}\infty} \left(1 - \exp \left(-\frac{u_r \cos \theta}{\langle\bar{u}\rangle_i} \frac{x - L_i}{d_i} \right) \right) = \langle\bar{c}\rangle_{\text{TBL}\infty} \left(1 - \exp \left(-\alpha \frac{x - L_i}{d_i} \right) \right), \quad (\text{B } 9)$$

thereby revealing that their coefficient $\alpha = (u_r \cos \theta) / \langle\bar{u}\rangle_i$ corresponds to a dimensionless bubble rise velocity. In order to solve Eqns. (B 8) or (B 9), the unknowns u_r and $\langle\bar{c}\rangle_{\text{TBL}\infty}$ need to be determined. One can perform some air-water flow measurements or, alternatively, use a best-fit approach.